Journal of Southeast University (English Edition) Vol. 28, No. 4, pp. 415 - 421 Dec. 2012 ISSN 1003—7985

Training image analysis for three-dimensional reconstruction of porous media

Teng Qizhi Yang Dan Xu Zhi Li Zhengji He Xiaohai

(School of Electronics and Information Engineering, Sichuan University, Chengdu 610065, China)

Abstract: In order to obtain a better sandstone three-dimensional (3D) reconstruction result which is more similar to the original sample, an algorithm based on stationarity for a two-dimensional (2D) training image is proposed. The second-order statistics based on texture features are analyzed to evaluate the scale stationarity of the training image. The multiple-point statistics of the training image are applied to obtain the multiple-point statistics stationarity estimation by the multi-point density function. The results show that the reconstructed 3D structures are closer to reality when the training image has better scale stationarity and multiple-point statistics stationarity by the indications of local percolation probability and two-point probability. Moreover, training images with higher multiple-point statistics stationarity and lower scale stationarity are likely to obtain closer results to the real 3D structure, and vice versa. Thus, stationarity analysis of the training image has far-reaching significance in choosing a better 2D thin section image for the 3D reconstruction of porous media. Especially, high-order statistics perform better than low-order statistics.

Key words: three-dimensional reconstruction; training image; stationarity; porous media; multiple-point statistics

doi: 10.3969/j.issn.1003-7985.2012.04.008

The reconstruction of three-dimensional (3D) porous media is of great help to have an accurate 3D reconstruction of the microstructure as input to computer models in clarifying and quantifying material properties that are difficult to obtain experimentally. The focus on 3D reconstruction algorithms has been on implementing reproduction based on the 2D image to generate realizations using different spatial information patterns[1-4]. For instance, the fast Fourier transform (FFT) algorithm employs statistical information of porosity and autocorrelation functions from 2D images[2]. The two-point autocorrelation function is often used as a reconstruction condition in the simulated annealing algorithm[5-6]. The multiple-point geology statistics method which extracts the configuration patterns from 2D images has become a popular reconstruction algorithm in recent years[7-8]. In conclusion, the statistical feature plays an important role in structure reproduction as a bridge between 2D images and 3D realizations, regardless of the mathematical representation.

As a commonly used concept in multiple-point geostatistics, a training image is the database of geological patterns in various forms. But to be a training image, a 2D image must satisfy a crucial condition, namely, the property of stationarity[9]. Stationarity means that the features and properties of the structure are independent of the location and size; that is, the distribution of the structure inside the sub-region of the training image does not change when the sub-region is shifted[10]. The assumption of stationarity about the training image must be ensured before 3D reconstruction. Otherwise, the stochastic simulation of the spatial information will be impossible.

As far as we know, there has been no relevant research on selecting training images in China up to now. Though some foreign literature takes that into account, porosity is the only parameter used for the selection of training images[11]. Actually, porosity is not a suitable representation of the features and properties of the structure information, since it is possible for images with the same porosity to have big differences in structures. Mirowski et al.[12] provided an analytical method of training images for multi-point geostatistics based on orientation, texture features and categories of the images. Since 3D reconstruction for porous media focuses on pores and grains, binary images are generally used as training images for reconstruction realization. Then orientation and category-based methods become inapplicable. In this paper, both the texture features and the multi-point statistics are employed as assessments of the stationarity of training images. As indicated by experiments that human perception is sensitive to the second-order statistics, the second-order analysis of images, e.g. the gray level co-occurrence matrix (GLCM), becomes a well-known method for image analysis[13]. Furthermore, the multiple-point statistics (MPS) contains higher-order statistics for 3D reconstruction. A process of stationarity assumption of the MPS is of great significance.

In this paper, the scale stationarity is introduced based on the texture features to analyze the second-order spatial information of the training image. Then, a high-order

Received 2012-06-28.

Biography: Teng Qizhi (1961—), female, doctor, professor, qzteng@scu.edu.cn.

Foundation item: The National Natural Science Foundation of China (No. 60972130).

Citation: Teng Qizhi, Yang Dan, Xu Zhi, et al. Training image analysis for three-dimensional reconstruction of porous media [J]. Journal of Southeast University (English Edition), 2012, 28(4): 415 - 421. [doi: 10.3969/j.issn.1003-7985.2012.04.008]

statistics method based on the multi-point density function (MPDF)[14] is followed for the MPS stationarity analysis. The scale stationarity score and MPS stationarity score on the 2D training image are obtained for the 3D reconstruction of porous media. Finally, the property of the reconstructed 3D pore structure is evaluated with local percolation probability and two-point probability to test the significance of the methods for the selection of training images.

1 Proposed Method

To evaluate the stationarity of the training image for 3D pore structure reconstruction, a method based on textural analysis and multiple-point statistics is proposed. The method consists of scale stationarity estimation and MPS stationarity estimation.

1.1 Scale-stationarity estimation of training image

The second-order texture feature is used to estimate the scale-stationarity of the training image. The training image is divided into nine overlapping sub-regions. The size of each region is chosen to be 1/4 of the whole image area (see Fig. 1). One of these sub-regions is extracted as the reference pattern, to which scale transforms are applied.

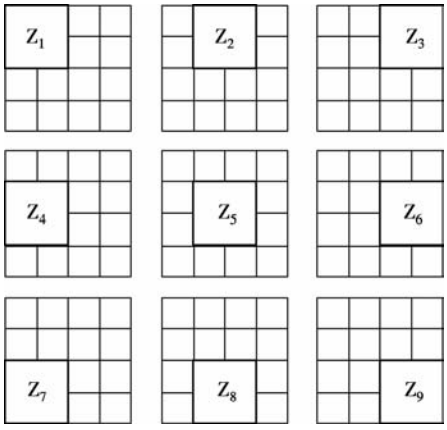

Fig. 1 Nine sub-blocks in training image

The gray level co-occurrence matrix (GLCM) method is used for extracting the second-order statistical information. It is a matrix of which the element means the relative frequency for two pixels, with intensity i and j respectively, occurring at a displacement distance within a given neighborhood. We usually have four angular gray level co-occurrence matrices for a given distance.

Haralick et al.[15] proposed 14 statistical features extracted from the GLCM and four most relevant features are selected to reduce the computational complexity[16]. These four features are energy E, entropy H, contrast C and inverse difference moment I, respectively. They are computed from each co-occurrence matrix using the following formulae:

$$E = \sum_{i=0}^{G-1}\sum_{j=0}^{G-1}[p(i,j)]^2 \tag{1}$$

$$H = -\sum_{i=0}^{G-1}\sum_{j=0}^{G-1}p(i,j)\log_2[p(i,j)] \tag{2}$$

$$C = \sum_{i=0}^{G-1}\sum_{j=0}^{G-1}(i-j)^2 p(i,j) \tag{3}$$

$$I = \sum_{i=0}^{G-1}\sum_{j=0}^{G-1}\frac{p(i,j)}{1+(i-j)^2} \tag{4}$$

where $p(i, j)$ is an element of the co-occurrence matrix which means the probability of the occurrences for the pixel pair (i, j); and (i, j) corresponds to the pair of gray levels i and j; G is the number of gray levels.

Two procedures are processed at the beginning of scale stationarity estimation as follows:

1) A series of scale factors or deformation parameters are applied to the reference pattern (extracted in Fig. 1). Parameter $a(x, y)$ is the scale factor along the x and y axes. Then we obtain the vector $\boldsymbol{V}_{\mathrm{RP},\ a(x,y)}$, which is the texture feature vector computed over the deformed reference pattern.

2) The other procedure is to compute vector $\boldsymbol{V}_{1,\ x,\ y}$, which is the texture feature vector computed over each sliding window as shown in Fig. 1, with the same size of the reference pattern. The sliding window in this flow has no deformation, which means that the scale factor $a(x, y) = (1, 1)$.

Then the Euclidian distance between these two vectors is calculated. For different locations of the sliding windows and different scale transformed reference patterns, we have Euclidian distances between $\boldsymbol{V}_{1,\ x,\ y}$ and $\boldsymbol{V}_{\mathrm{RP},\ a(x,y)}$. For each sliding window, the minimum Euclidian distance derives a scale factor $a(x, y)$ as follows:

$$a(x,y) = \underset{a(x,y)}{\operatorname{argmin}}\left\{\sum_{i=0}^{N}[\boldsymbol{V}_{1,x,y}(i) - \boldsymbol{V}_{\mathrm{RP},a(x,y)}(i)]^2\right\} \tag{5}$$

where $a(x, y)$ is the best scale factor; N is the number of elements in the vectors $\boldsymbol{V}_{1,\ x,\ y}$ or $\boldsymbol{V}_{\mathrm{RP},\ a(x,y)}$, containing $N = 4 \times 4 = 16$ elements, namely four GLCM elements in four different angle directions.

Nine minimum Euclidian distance dilation factor couples $a(x, y)$ yield a best affinity map, i.e., the best matches between the sliding window and the reference pattern. The spread of the points p_1, p_2, …, p_n defined by the dilation factor couples is computed by the singular value decomposition (SVD):

$$\begin{bmatrix} x_i \\ y_i \end{bmatrix}_{i\in[1,n]} = \boldsymbol{U}\times\boldsymbol{S}\times\boldsymbol{V}^{\mathrm{T}} \tag{6}$$

where $\boldsymbol{S}$ is the augmented diagonal matrix with entries s_1, s_2, while $\boldsymbol{U}$ and $\boldsymbol{V}$ are the orthonormal matrices. The parameters x_i and y_i are associated with the cloud of point p_n, through a bijection in order to transform the dilation factor into the scale-space for principal component analysis[17]. To be more specific, the dilation factors 1/2, 2/3, 3/4,

1, 4/3, 3/2, 2 along the x axis and y axis are mapped to −1, −2/3, −1/3, 0, 1/3, 2/3, 1, respectively.

The scale stationarity score S_1 for the image is defined as

$$S_1 = 1 - \min\left\{1, D_u\left(1 + \frac{s_2}{s_1}\right)\right\} \tag{7}$$

where s_1, s_2 are singular values obtained from Eq. (6) and u_i is the coordinate of p_1, p_2, …, p_n along the first principal direction according to the SVD. Parameter D_u is the variability along the first principal direction:

$$D_u = \sqrt{\frac{1}{n-1}\sum_{j=1}^{n}(u_j - \bar{u})^2} \qquad \bar{u} = \frac{1}{n}\sum_{i=1}^{n} u_i \tag{8}$$

1.2 MPS stationarity estimation of the training image

The multiple-point statistics describe the configuration pattern of the image indicating the probability of particular multiple-point statistics occurrence. Before reconstructing the 3D pore structure, statistical information of the 2D training images must be properly represented with particular functions. The representation of high-order statistical information is one of the necessary issues. The MPDF characterizes the frequency of a specific multiple-point configuration. As porous media is usually considered as two phases, there is a total of 16 (2^4) different configurations for a four-point configuration (see Fig. 2), 32 (2^5) for five-point configurations and so on.

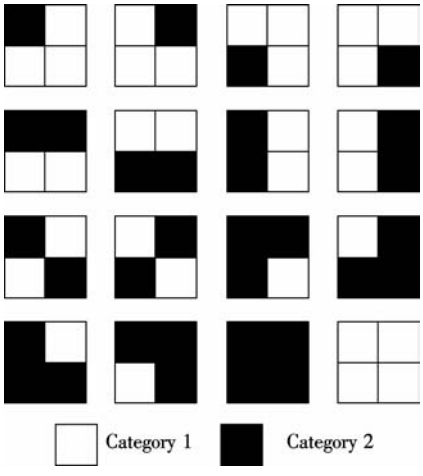

Fig. 2 Possible combinations of two categories for a square four-point configuration

Taking four-point configurations into account, the multiple-point density function is obtained by counting the number of times that each configuration in Fig. 2 occurs in an image, which means the probability of the configurations in the image.

The MPS stationarity estimation method is based on the multiple-point density function. The training image is also divided into nine sub-regions as mentioned in section 1.1. The MPDF is calculated over these sub-regions. The MPDF of the whole training image is also computed as the reference.

For each sub-region, we analyze the sum of the absolute difference of the multiple-point density function between the sub-region and the whole training image. The sum is defined as

$$\Delta_j = \sum_{i=1}^{n} |f_0(i) - f_1(i,j)| \tag{9}$$

where n is the number of configuration arrangement events; $f_0(i)$ is the frequency corresponding to configuration i in the whole training image; and $f_1(i,j)$ is the frequency corresponding to configuration i in sub-region j.

The smaller the sum of absolute difference indicates a better similarity between two multiple-point distributions. The variability of the sums of absolute differences characterizes the similarity between different sub-blocks in the training image as follows ($\bar{\Delta}$ is the mean value of parameters Δ_j):

$$D_\Delta = \sqrt{\frac{1}{n-1}\sum_{j=1}^{n}(\Delta_j - \bar{\Delta})^2} \qquad \bar{\Delta} = \frac{1}{n}\sum_{i=1}^{n}\Delta_i \tag{10}$$

Then MPS-stationarity score S_2 for the image is defined as

$$S_2 = 1 - D_\Delta \tag{11}$$

2 Experimental Results and Discussion

In order to verify the effectiveness of the method for 3D reconstruction, the training images that have different stationarity scores are used to generate 3D structures through different reconstruction algorithms, such as the simulated annealing (SA) and the multiple-point geology statistics method. Four training images are randomly selected from a serial of micro-CT images with the size of 128 × 128 × 128 and the resolution of 30 μm/pixel. Meanwhile, the micro-CT images are tested as a reference of the results.

Fig. 3 shows four different 2D image samples. The scale stationarity score of sample_1 (see Fig. 3(a)) is 0.669 385 and that of sample_2 (see Fig. 3(b)) is 0.055 267, while the MPS stationarity scores are 0.963 920 and 0.889 441, respectively. Most training images with larger scores of scale stationarity have larger MPS stationarity scores, and there are a few images which have larger scores of scale stationarity but smaller MPS stationarity scores. The scale stationarity scores of sample_3 (see Fig. 3(c)) and sample_4 (see Fig. 3(d)) are 0.602 321 and 0.015 143, respectively; while the MPS stationarity scores are 0.892 314 and 0.943 563, respectively. These images are used as training images for 3D reconstruction employing different algorithms as mentioned in the previous section. By calculating the local percolation probability and the two-point probability, we analyze and compare the properties of the reconstructed 3D realizations in

the following section.

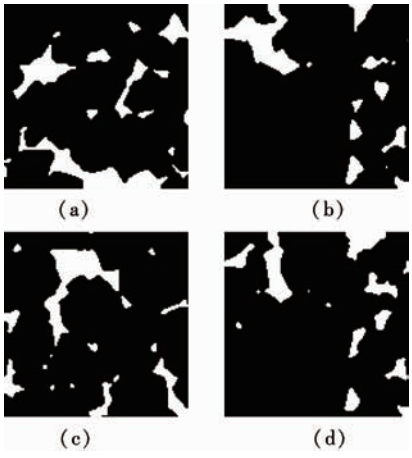

Fig. 3 Training images with different stationarity scores. (a) Sample_1; (b) Sample_2; (c) Sample_3; (d) Sample_4

2.1 Local percolation probability

The local percolation probability measures the connectivity of measurement cells with a given local porosity Φ. We define $K(r, L)$ as a measurement cell that denotes the cube centered at the lattice vector $\boldsymbol{r}$ with side-length L[18-19]. The percolation characteristic function is defined as

$$\Lambda_\alpha(\boldsymbol{r}, L) = \begin{cases} 1 & K(\boldsymbol{r}, L) \text{ percolates in } \alpha \text{ direction} \\ 0 & \text{otherwise} \end{cases} \quad (12)$$

where $\Lambda_\alpha(\boldsymbol{r}, L) = 1$ represents that fluid can percolate from one side to the other side of the measurement cell along α direction. Then the local percolation probability along α direction can be defined as

$$\lambda_\alpha(\Phi, L) = \frac{\sum_{\boldsymbol{r}} \Lambda_\alpha(\boldsymbol{r}, L)\delta(\Phi - \Phi)(\boldsymbol{r}, L))}{\sum_{\boldsymbol{r}} \delta(\Phi - \Phi)(\boldsymbol{r}, L))} \quad (13)$$

where the δ function means the range of Φ and $\Phi + \mathrm{d}\Phi$ in a measurement cell, and L is the side-length of the cell.

The distribution of the curves of the local percolation probabilities in different directions characterizes the connectivity and isotropy of the 3D pore structure qualitatively. The curves will overlap when $\lambda_\alpha(\Phi, L)$ are similar in the X, Y, Z directions, implying homogeneity, as the curves will gather when the property of the porous media has the trend to be isotropic. Meanwhile, faster increasing speeds of the curves mean better connectivity of the structure.

Fig. 4 shows the local percolation probability curves of the micro-CT images as a reference. Label "3" means the fluid percolates along all the three directions (X, Y and Z) while label "C" means the fluid percolates along any of the three directions. Fig. 5 and Fig. 6 present local percolation probability curves of the 3D pore structures reconstructed from sample_1 and sample_2 with two reconstruction methods, i.e., the SA algorithm and the MPS algorithm. Clearly, the local percolation probability curves of the 3D pore structures reconstructed from sample_1 imply better properties of isotropy and connectivity than those from sample_2.

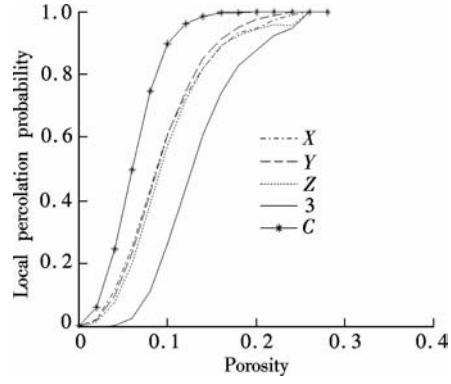

Fig. 4 Local percolation probability for the micro-CT images

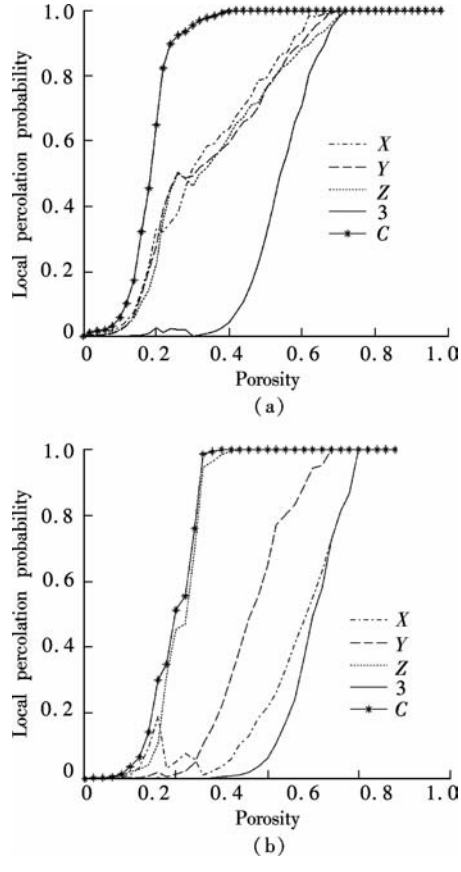

Fig. 5 Local percolation probability of 3D pore structure reconstructed from different samples by SA algorithm. (a) Sample_1; (b) Sample_2

Fig. 7 and Fig. 8 show the local percolation probability curves of 3D realizations reconstructed from sample_3 and sample_4 by two reconstruction methods. Sample_3 has a larger scale stationarity score but a smaller MPS stationarity score than sample_4. Results of Fig. 7 and Fig. 8 show that the local percolation probability curves of 3D pore structures reconstructed from sample_4 indicate better properties of isotropy or connectivity than those from sample_3, which means training images with a larger MPS stationarity score is better for 3D reconstruction.

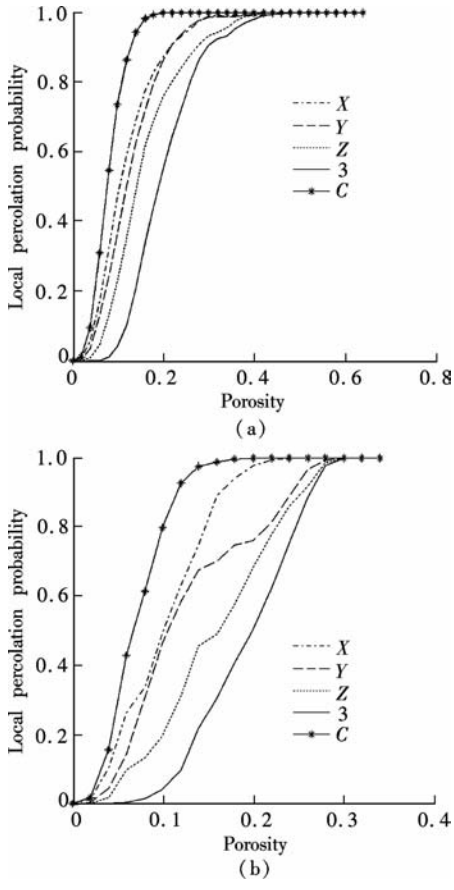

Fig. 6 Local percolation probability of 3D pore structure reconstructed from different samples by MPS algorithm. (a) Sample_1; (b) Sample_2

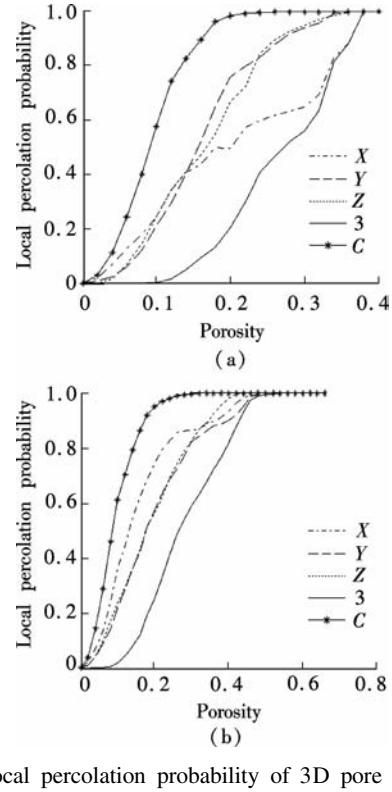

Fig. 7 Local percolation probability of 3D pore structure reconstructed from different samples by SA algorithm. (a) Sample_3; (b) Sample_4

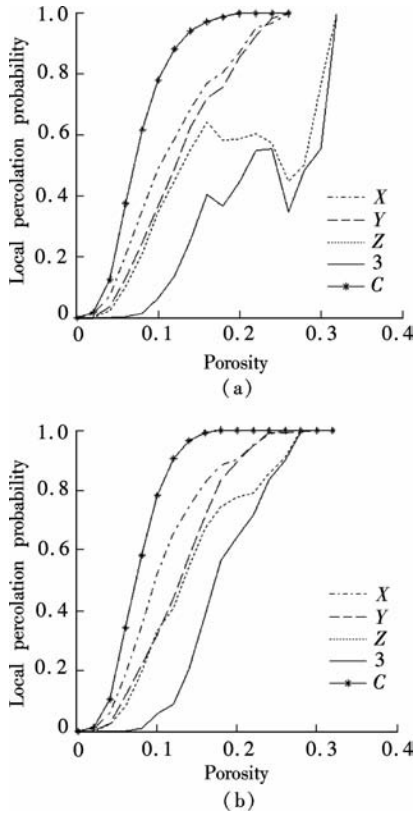

Fig. 8 Local percolation probability of 3D pore structure reconstructed from different samples by MPS algorithm. (a) Sample_3; (b) Sample_4

2.2 Statistic characteristics

Two-point probability describes the probability of two pixels in the same phase occurring at a specific distance. In Fig. 9 and Fig. 10, Curves of the two-point probability of the 3D structures reconstructed using the SA and MPS reconstruction algorithms are compared with the two-point probability of the real micro-CT images. Reconstructed structures of Figs. 3(a), (b), (c) and (d) are denoted as 0040, 0108, 0015 and 0105, respectively, according to the serial number of the training images in real micro-CT images. Curves of the two-point probability for these reconstructed 3D pore structures are compared with those from the realistic porous media. As shown in Fig. 9, it is obvious that the two-point probability function curves of sample_1 are closer to the curves acquired from the real micro-CT images than those of sample_2. This confirms that training images with a larger scale stationarity score and a MPS stationarity score are better for 3D reconstruction. Fig. 10 shows the curves of sample_3 and sample_4. Obviously, the two-point probability property of the structures from sample_4 is more similar to the property of the micro-CT image than that from sample_3. This result is consistent with the experimental results in section 2.1, which means that the MPS stationarity score can indicate a better training image, while the scale stationarity score may be invalid in a few cases.

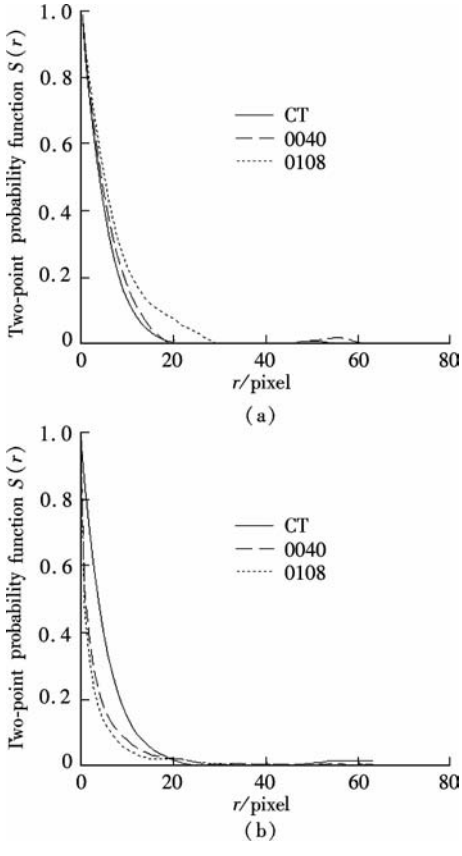

Fig. 9 Two-point probability functions $S(r)$ of the 3D pore structure reconstructed from sample_1 and sample_2 with different methods. (a) SA algorithm; (b) MPS algorithm

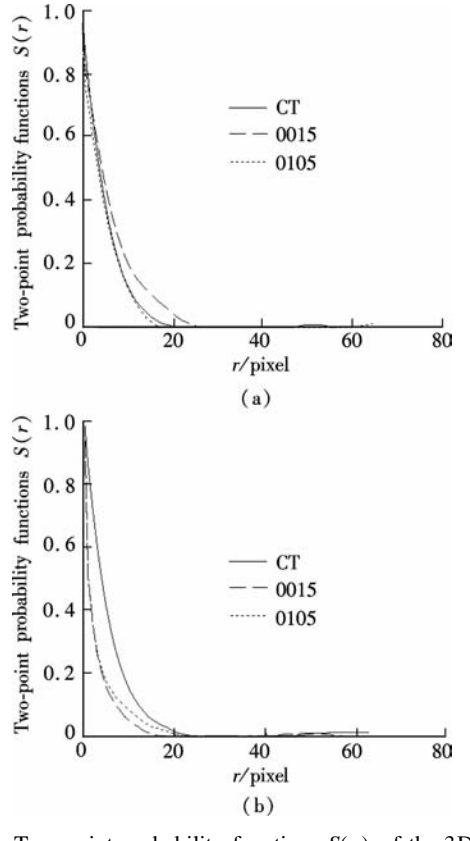

Fig. 10 Two-point probability functions $S(r)$ of the 3D reconstructed structures from sample_3 and sample_4 with different methods. (a) SA algorithm; (b) MPS algorithm

3 Conclusion

In this paper, a spatial information analysis is implemented for the training image before 3D pore structure reconstruction of porous media. Multi-scale analysis and principal component analysis are used to evaluate the scale stationarity based on the texture feature. Furthermore, the absolute difference of the multiple-point density function is applied to characterize the multi-point statistics stationarity for the training image. Stationarity scores obtained by the methods decide the better 2D training image for the 3D reconstruction of the porous media. Two different reconstruction algorithms are used to verify our theory, with the real micro-CT images as reference. According to the obtained results, it is confirmed that training images with larger stationarity scores will lead to better reconstruction results of porous media. Meanwhile, it is noticed that better MPS stationarity performance usually implies better 3D reconstruction results while the scale stationarity method may be invalid in a few cases, which is obvious since multiple point statistics actually contain all the lower order statistics.

References

[1] Tang T, Teng Q Z, He X H, et al. A pixel selection rule based on the number of different-phase neighbours for the simulated annealing reconstruction of sandstone microstructure [J]. *Journal of Microscopy*, 2009, **234**(3): 262 – 268.

[2] Liang Z R, Fernandes C P, Magnani F S, et al. A reconstruction technique for three-dimensional porous media using image analysis and Fourier transforms [J]. *Journal of Petroleum Science and Engineering*, 1998, **21**(3/4): 273 – 283.

[3] Tahmasebi P, Hezarkhani A, Muhammad S. Multiple-point geostatistical modeling based on the cross-correlation functions [J]. *Computational Geosciences*, 2012, **16**(3): 779 – 797.

[4] Čapek P, Hejtmánek V, Brabec L, et al. Stochastic reconstruction of particulate media using simulated annealing: improving pore connectivity [J]. *Transport in Porous Media*, 2009, **76**(2): 179 – 198.

[5] Liu X F, Sun J M, Wang H T. Reconstruction of 3-D digital cores using a hybrid method [J]. *Applied Geophysics*, 2009, **6**(2): 105 – 112.

[6] Jiao Y, Stillinger F H, Torquato S. Modeling heterogeneous materials via two-point correlation functions. Ⅱ. algorithmic details and applications [J]. *Physical Review E*, 2008, **77**(3): 031135.

[7] Strebelle S. Conditional simulation of complex geological structures using multiple-point statistics [J]. *Mathematical Geology*, 2002, **34**(1): 1 – 21.

[8] Hajizadeh A, Safekordi A, Farhadpour F A. A multiple-point statistics algorithm for 3D pore space reconstruction from 2D images [J]. *Advances in Water Resources*, 2011, **34**(10): 1256 – 1267.

[9] Caers J, Zhang T. Multiple-point geostatistics: A quanti-

tative vehicle for integrating geologic analogs into multiple reservoir models [C]//*Integration of Outcrop and Modern Analogs in Reservoir Modeling*. Tulsa: American Association of Petroleum Geologists, 2004: 383 - 394.

[10] Illian J, Penttinen A, Stoyan H, et al. *Statistical analysis and modeling of spatial point patterns* [M]. Chichester: John Wiley & Sons, 2008: 173 - 291.

[11] Okabe H, Blunt M J. Pore space reconstruction using multiple-point statistics [J]. *Journal of Petroleum Science and Engineering*, 2005, **46**(1/2): 121 - 137.

[12] Mirowski P W, Tetzlaff D M, Davies R C, et al. Stationarity scores on training images for multipoint geostatistics [J]. *Mathematical Geosciences*, 2009, **41**(4): 447 - 474.

[13] Prats-Montalbán J M, de Juan A, Ferrer A. Multivariate image analysis: A review with applications [J]. *Chemometrics and Intelligent Laboratory Systems*, 2011, **107**(1): 1 - 23.

[14] Boisvert J B, Pyrcz M J, Deutsch C V. Multiple-point statistics for training image selection [J]. *Natural Resources Research*, 2008, **16**(4): 313 - 321.

[15] Haralick R M, Shanmugam K, Dinstein I. Textural features for image classification [J]. *IEEE Trans on Systems, Man, and Cybernetics*, 1973, SMC-**3**(6): 610 - 621.

[16] Manivannan K, Aggarwal P, Devabhaktuni V, et al. Particulate matter characterization by gray level co-occurrence matrix based support vector machines [J]. *Journal of Hazardous Materials*, 2012, **223/224**: 94 - 103.

[17] Abdi H, Williams L J. Principal component analysis [J]. *Wiley Interdisciplinary Reviews*: *Computational Statistics*, 2010, **2**(4): 433 - 459.

[18] Latief F D E, Biswal B, Fauzi U, et al. Continuum reconstruction of the pore scale microstructure for Fontainebleau sandstone [J]. *Physica A*: *Statistical Mechanics and Its Applications*, 2010, **389**(8): 1607 - 1618.

[19] Hu J, Stroeven P. Local porosity analysis of pore structure in cement paste [J]. *Cement and Concrete Research*, 2005, **35**(2): 233 - 242.

多孔介质三维重建的训练图像分析

滕奇志 杨 丹 徐 智 李征骥 何小海

(四川大学电子信息学院, 成都 610065)

摘要:为了使砂岩三维重建结果更接近于原始样本,提出了一种基于平稳性的二维训练图像分析方法. 基于纹理特征分析了训练图像的二阶统计特征以获取尺度平稳性;通过多点密度函数分析训练图像的多点统计特征,获取多点统计平稳性. 实验结果表明:对于尺度平稳性和多点统计平稳性都相对较高的训练图像,重建得到的三维结构的局部渗透性和两点统计概率特性更接近于真实三维结构的相关特性. 而多点统计平稳性较高但尺度平稳性较低的训练图像,与多点统计平稳性较低而尺度平稳性较高的训练图像相比,更接近于真实三维图像. 因此,训练图像的平稳性评估对于三维重建的二维薄片图像选取具有重要作用,同时,高阶统计分析方法更为准确.

关键词:三维重建;训练图像;平稳性;多孔介质;多点统计

中图分类号:TE319